Journal of Power Sources 270 (2014) 342–348

Contents lists available at ScienceDirect

Journal of Power Sources

journal homepage: www.elsevier.com/locate/jpowsour

Effects of hydrophobic agent content in macro-porous substrates on the fracture behavior of the gas diffusion layer for proton exchange membrane fuel cells

Sanwi Kim [a], Byeong-Heon Jeong [b], Bo Ki Hong [b, **], Taek-Soo Kim [a, *]

[a] Department of Mechanical Engineering, KAIST, Daejeon 305-701, Republic of Korea
[b] Fuel Cell Vehicle Team 1, Eco-Technology Center, Research & Development Division, Hyundai-Kia Motors Company, Yongin-si, Gyeonggi-do 446-716, Republic of Korea

HIGHLIGHTS

- Adhesion between MPS and MPL of a GDL has been measured for the first time.
- Adhesion enhancement mechanism was discovered by OM, SEM, and EDX.
- Higher PTFE contents in MPS led to better interaction between MPL and MPS.

ARTICLE INFO

Article history:
Received 23 May 2014
Received in revised form
11 July 2014
Accepted 20 July 2014
Available online 25 July 2014

Keywords:
Gas diffusion layer
Interfacial fracture energy
Double cantilever beam fracture mechanics test
Proton exchange membrane fuel cell

ABSTRACT

Although the adhesion between the macro-porous substrate (MPS) and micro-porous layer (MPL) of a gas diffusion layer (GDL) is a critical factor that affects the reliability and durability of proton exchange membrane fuel cells, systematic studies quantifying the interfacial fracture energy of GDL have not yet been reported. Therefore, in this study, the interfacial fracture energy of GDLs with different contents of hydrophobic agents in the MPS is quantitatively measured. GDL samples with 0, 5, 10, and 20 wt% of hydrophobic agent content are tested using double cantilever beam fracture mechanics tests. It is observed that the interfacial fracture energy of the GDLs increases as the content of hydrophobic agent increases, due to more favorable interactions between the hydrophobic agents of the MPL and MPS. Optical microscope, scanning electron microscope, and energy-dispersive X-ray spectroscope analyses are performed on the bare and delaminated surfaces in order to investigate the mechanism of the interfacial fracture energy increase of the GDLs.

1. Introduction

Due to the numerous advantages of proton exchange membrane fuel cells (PEMFCs), such as high power density, high efficiency, low operation temperature, low pollution, and low noise, they have been garnering significant attention for a wide range of applications including transportation, stationary, and portable applications [1–4]. Still, some issues must be resolved before PEMFC technology can be successfully applied in commercial uses. Researchers have focused on many PEMFC issues in order to improve its technology for better commercialization. These research topics have included performance improvement, durability, water management, and cost competitive materials [5–8]. More specifically, the membrane electrode assembly (MEA) and gas diffusion layer (GDL) are two critical components of PEMFCs that have been examined extensively in both academia and industry.

The GDL is typically composed of a micro-porous layer (MPL) and a macro-porous substrate (MPS) or backing [9–11]. In general, the MPL consists of carbon black powder and hydrophobic agent such as polytetrafluoroethylene (PTFE) or fluorinated ethylene-propylene [12,13]. The MPL provides better reactant gas transport and excessive water removal for PEMFCs and lowers the electrical contact resistance between the catalyst layer and GDL [14]. In contrast, the MPS is composed of hydrophobic agent and carbon fibers in the form of felt, paper, or cloth [15]. The MPS also has an important function in physically supporting the MEA, providing

* Corresponding author. Tel.: +82 42 350 3238; fax: +92 42 350 3210.
** Corresponding author. Tel.: +82 31 899 3202; fax: +82 31 368 3331.
E-mail addresses: boki.hong@hyundai.com (B.K. Hong), tskim1@kaist.ac.kr (T.-S. Kim).

http://dx.doi.org/10.1016/j.jpowsour.2014.07.122
0378-7753/

electron paths for flows between the catalyst layer and bipolar plate, and removing the excessive product water [16–18]. These GDL features should function well in order to improve the overall efficiency of PEMFCs, however, previous experiences in both academic and industrial fields have demonstrated that GDLs have weak fracture qualities and break very easily. Therefore, for the past decade, extensive studies have been conducted in order to investigate the long-term durability of the key components of PEMFCs, such as the MEAs and GDLs [19–22]. More efficient assessment of the critical parameters that affect the long-term durability of the fuel cell components under freeze-thaw or dry-wet cycling conditions is crucial to the commercialization of fuel cell vehicles because the conventional durability tests are costly and very time-consuming, i.e. up to several months. Thus, a deeper understanding of the fracture behavior of the MEA and GDL is very important in estimating the long-term durability of the components in actual fuel cells. Recently, Jia et al. [23] reported the effects of contamination and relative humidity (RH) on the fracture behavior of MEAs. On the other hand, systematic studies quantifying the adhesion strength between the MPL and MPS of the GDL in terms of interfacial fracture energy have not yet been undertaken and the primary factor in the fracture behavior has not been elucidated.

Therefore, in this study, a novel testing procedure for quantitatively measuring the interfacial fracture energy of the GDL is established using a double cantilever beam (DCB) fracture mechanics testing method. Then, this method is applied to several GDL samples in order to elucidate the effects of the hydrophobic agent content in the MPS on the interfacial fracture energy of the GDL.

2. Experimental

2.1. Materials and morphology characterization

In order to measure the interfacial fracture energy of the GDLs, four commercial carbon fiber felt-based GDLs (10AC, 10BC, 10CC, and 10DC) with different amounts of PTFE hydrophobic agent in the MPS (0, 5, 10, and 20 wt%, respectively) were obtained from SGL Technologies GmBH, Germany. An identical 'C'-type MPL was applied to all the four GDLs in this study and the PTFE content in the 'C'-type MPL is known to be 22.5 ± 2.5 wt% [24,25]. The thickness of each GDL sample was reported as the average and standard deviation values of 20 individual measurements using a digital micrometer (Mitutoyo Co., Japan). The key characteristics of the GDL samples, such as the GDL thickness, MPL presence, MPS type, and PTFE content in the MPS are listed in Table 1. Furthermore, in order to thoroughly examine the surface morphology of the GDLs, both an optical microscope (OM; Digital Microscope VHX-1000 Model, Keyence, Japan) and a scanning electron microscope (SEM; FE-SEM Sirion Model, FEI, USA) were used in this study.

All GDL samples in this study were composed of both MPLs and MPSs, and their morphologies for all GDLs used in this study were observed by SEM in Fig. 1(a–d). The same MPL that was also wet-proofed via a PTFE hydrophobic treatment was used for the four GDL samples. As explained in the introduction, the microstructure of the GDL is generally recognized as a combination of MPL and MPS. Technically speaking, however, there is an interfacial region between the MPL and MPS phases (i.e. a mixed layer) that is composed of mixed phases of both MPL and MPS as seen in Fig. 1(e) and (f). It was observed that the thickness of the mixed layer was relatively thick, and the border between the MPL and MPS phases was not clearly distinguishable.

Table 1
Key characteristics of the GDL samples.

GDL sample name	GDL grade name	GDL thickness (μm)	MPL presence	MPS type	Content of PTFE in MPS (wt%)
GDL-0	10AC	410 ± 8	Yes	Carbon fiber felt	0
GDL-5	10BC	436 ± 5	Yes	Carbon fiber felt	5
GDL-10	10CC	428 ± 5	Yes	Carbon fiber felt	10
GDL-20	10DC	425 ± 7	Yes	Carbon fiber felt	20

2.2. DCB test method

The DCB test is a fracture mechanics testing method that allows accurate quantitative measurement of the critical value of the strain energy release rate or fracture energy. In order to measure the interfacial fracture energy of the GDL specimens, the DCB test method was introduced in this study, and Fig. 2(a) and (b) present the schematics of the DCB specimen. The GDL samples were cut into the dimensions of 10 mm (width) by 40 mm (length) using a sharp razor blade. All GDL specimens for the DCB testing were cut carefully in order that the length direction of the GDL specimen was in parallel with the machine direction of the GDL roll. The rectangular GDL specimens were sandwiched by 3 mm thick polycarbonate (PC) substrates, as described in Fig. 2(a). Different adhesives were used to attach the GDL specimens to the polycarbonate, depending on whether the adjoining surface was MPL or MPS. For the MPL side, Epo-Tek 353ND (consisting of bisphenol F and imidazole; Epoxy Technology Co., USA) with a low viscosity was used, while 3M Scotch-Weld™ DP-420 (consisting of 2,4,6-tris((dimethylamino)methyl) phenol; 3M Co., USA) with high viscosity was used for the MPS side. The different adhesives were used due to the very different surface characteristics of the MPL and MPS. Compared with the MPL, the MPS surface contains relatively large pores (approximately several tens of micrometers) because it is primarily composed of carbon fiber felts, however, the MPL surface contains very small pores (less than micrometer-scale) and some small cracks. In order to induce a clear interfacial fracture path, the adhesives must penetrate into the MPL and MPS layers to a certain depth. Therefore, a low viscosity adhesive (353ND) is suitable for the MPL with small pores and cracks, while a high viscosity adhesive (DP-420) is suitable for the MPS with large pores.

Once the adhesives were applied to the PC substrates and the GDL specimen was sandwiched between the two PC substrates, a constant clamping pressure of 150 kPa was applied to the entire sandwiched unit followed by a curing process at 120 °C for 2 h in a convection oven. After curing the DCB test specimen, aluminum loading tabs were attached on top of the PC substrate surfaces using a commercial epoxy adhesive (DP-420), as illustrated in Fig. 2(b).

The DCB test was conducted using a high-precision micromechanical test system (Delaminator Adhesion Test System; DTS Co., USA). Fig. 3 presents the schematic of the DCB testing system used in this study. This test system was constructed of a linear actuator, loading grips, and a load cell (see Fig. 3(a)). The aluminum loading tabs attached to the DCB specimen structure were linked to the loading grip using steel pins (see Fig. 3(b)). This test procedure has been used extensively to measure the interfacial fracture energy of thin film structures [26–34]. During the DCB test, the specimen was loaded and unloaded under a constant displacement rate of approximately 2.5 μm s^{-1}. The constant displacement rate was determined using the range of other published papers [31,33].

3. Results and discussion

In the DCB tests of the GDL specimens, the crack length (a) and the interfacial fracture energy (G_c) can be calculated using the following equations [27,28]. In Eq. (2), G_c is defined as the critical value of the applied strain energy release rate (G):

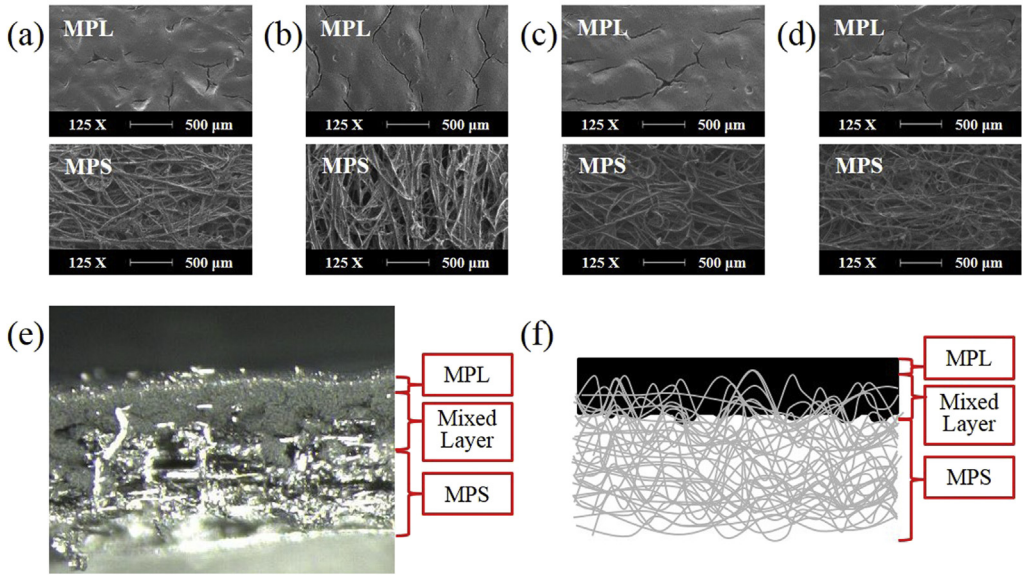

Fig. 1. Morphology of the GDLs: surface morphology of (a) GDL-0, (b) GDL-5, (c) GDL-10, and (d) GDL-20 by SEM; (e) cross-sectional morphology of the GDL-5 by OM; (f) a schematic illustration of the cross-sectional morphology of the GDL.

$$a = \left(\frac{du}{dP}\frac{E'bh^3}{8}\right)^{\frac{1}{3}} - 0.64h, \quad (1)$$

$$G = \frac{12P^2a^2}{E'b^2h^3}\left(1 + 0.64\frac{h}{a}\right)^2, \quad (2)$$

where P is the applied load, E' is the plane strain modulus of the beam, b is the specimen width, h is the half height of the specimen, and u is the DCB opening displacement. In order to measure several crack lengths and their corresponding fracture energies from a single test, several loading and unloading cycles were performed.

The fracture energies measured using the DCB test for different GDL samples are presented in Fig. 4. The results demonstrate that the interfacial fracture energy increases gradually as the PTFE content increases. For the GDL with 0 wt% PTFE (GDL-0), the interfacial fracture energy was measured to be 17.0 ± 1.5 J m^{-2}. The interfacial fracture energy of the GDL with 5 wt% PTFE (GDL-5) significantly increased to 39.6 ± 4.3 J m^{-2}, but a slight decrease in the interfacial fracture energy (37.9 ± 7.6 J m^{-2}) was observed for the GDL with 10 wt% PTFE (GDL-10). Nevertheless, when considering the fluctuation range of the measured value, the interfacial fracture energy of the GDL with 10 wt% PTFE appeared to be substantially similar to that with 5 wt% PTFE. The exact reason for this fracture behavior is not yet fully understood, but one possible reason is that as long as the MPS contains a certain amount of PTFE, i.e. at least 5 wt%, a further slight increase in the PTFE content to 10 wt% does not significantly affect the adhesion strength between the MPL and MPS, which leads to somewhat leveling-off trend. On the other hand, there was a subsequent large increase in the PTFE content from 10 to 20 wt% (GDL-20): the interfacial fracture energy of the GDL increased to 53.3 ± 7.5 J m^{-2}, which is approximately three times higher than that of the GDL without PTFE in the MPS. Thus, the results indicate that the interfacial fracture energy of the GDL increases with increasing PTFE content in the MPS.

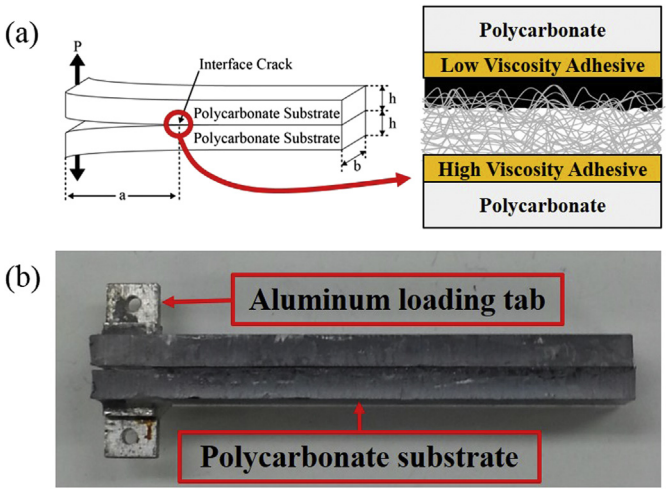

Fig. 2. (a) A schematic of the DCB specimen and (b) a photo of actual DCB specimen.

In order to understand the mechanism of the observed fracture behavior in more detail, the surface characterization on the delaminated GDL surfaces after the DCB tests was performed using the OM and SEM. Fig. 5 illustrates the delaminated surfaces of the GDL specimens with 0–20 wt% PTFE content in the MPS observed by the OM. The "MPL side" indicates the delaminated surface that primarily contains MPL, while the "MPS side" indicates the delaminated surface that primarily has MPS, which is also schematically explained in Fig. 5. From these OM images, the following phenomena were observed. When the two representative delaminated surfaces of GDL without any PTFE in MPS (GDL-0) and GDL with PTFE in MPS (GDL-20) were compared, it is clear that the GDL-20 has significantly more MPL residues between carbon fibers in the MPS than the GDL-0. The carbon fibers of the GDL-20 are barely visible due to the presence of the MPL residues surrounding each carbon fiber, while the carbon fibers of the GDL-0 were clearly visible, presumably due to the easy removal of the MPLs from the carbon fibers in the MPS. It should be noted that the OM images are suitable for the relative comparison of macroscopic morphology between GDL without any PTFE in MPS and GDL with PTFE in MPS. In order to examine the microscopic fracture surface, SEM has been used for more detailed observation of internal fractured surfaces.

The delaminated surfaces of all GDLs (GDL-0, 5, 10, and 20) were further examined via SEM, as seen in Fig. 6. The SEM images of the MPL and MPS sides were obtained for all GDLs. The carbon

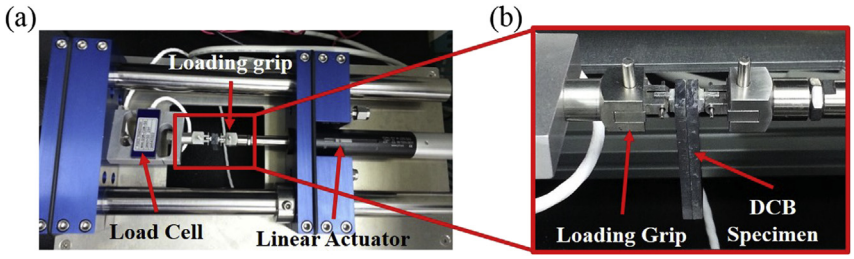

Fig. 3. A schematic of the DCB testing system: (a) a photo of the whole DCB testing system; (b) an enlarged photo of the specimen mounting part.

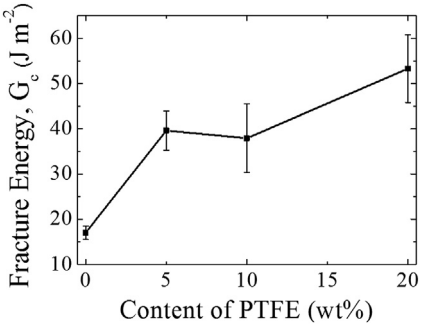

Fig. 4. Fracture energy of the GDL samples as a function of PTFE content in MPS.

fibers in the MPS are highlighted in blue (in web version) to easily distinguish them from the MPL residue. The results exhibit a clear difference in the morphology between the GDLs, which further supports the OM observations. For the MPL side morphology, it was observed that the GDLs with weak adhesion (such as GDL-0) exhibited clear traces of delaminated carbon fibers due to the easy separation or removal during the DCB test, while the GDLs with strong adhesion (such as GDL-20) exhibited relatively vague traces of delaminated carbon fibers due to the higher resistance of the fibers to the external forces exerted during the test. Subsequently, the MPS side morphology of the weak adhesion GDLs (such as GDL-0) also reflected the easy separation of the MPL from the carbon fibers in the MPS, which left few residual MPL traces on the fiber surfaces. On the other hand, the GDLs with strong adhesion (such as GDL-20) exhibited significantly more MPL residue on the carbon fibers, which indicates higher adhesion strength between the MPL and MPS. A possible mechanism for this observation is explained in Fig. 7. As already described in Fig. 6, the morphological observation via the SEM is in good agreement with that by the OM, which also strongly supported the interfacial fracture energy results in Fig. 4 and the debonding mechanism in Fig. 7. Therefore, the results in this study can be attributed to the higher PTFE content in the MPS facilitating more favorable interactions with the PTFE in the MPL, which leaves a significant amount of MPL residue on the surfaces of the carbon fibers; finally, this results in a higher interfacial fracture energy between the MPL and MPS of the GDL.

In order to further analyze the delaminated surfaces, energy-dispersive X-ray spectroscope (EDX) analyses were performed for the following surfaces, as seen in Fig. 8: the bare MPL, bare MPS, delaminated MPL side, and delaminated MPS side. The EDX analyses on the bare MPL (Fig. 8(a)) and MPS (Fig. 8(b)) were undertaken using a fresh GDL surface before the DCB test. For the delaminated MPL (Fig. 8(c)) and MPS (Fig. 8(d)) sides, the EDX analyses were performed for each delaminated surface after the DCB test. As expected, the contents of the carbon and fluorine elements in the bare MPL surfaces of the four GDLs remained constant, as seen in Fig. 8(a), because the same type of MPL was applied to all GDL samples explored in this study. For the bare MPS surfaces, the content of the fluorine elements increased with increases in the PTFE content in the MPS, whereas the content of carbon elements decreased accordingly, as seen in Fig. 8(b).

As illustrated in Fig. 8(c), the carbon and fluorine contents of the delaminated surfaces of the MPL sides were similar to those of the bare MPL surfaces, which indicate that the delaminated MPL sides do not contain significant amounts of carbon fibers. In Fig. 8(d), the carbon element contents of the delaminated surfaces of the MPS

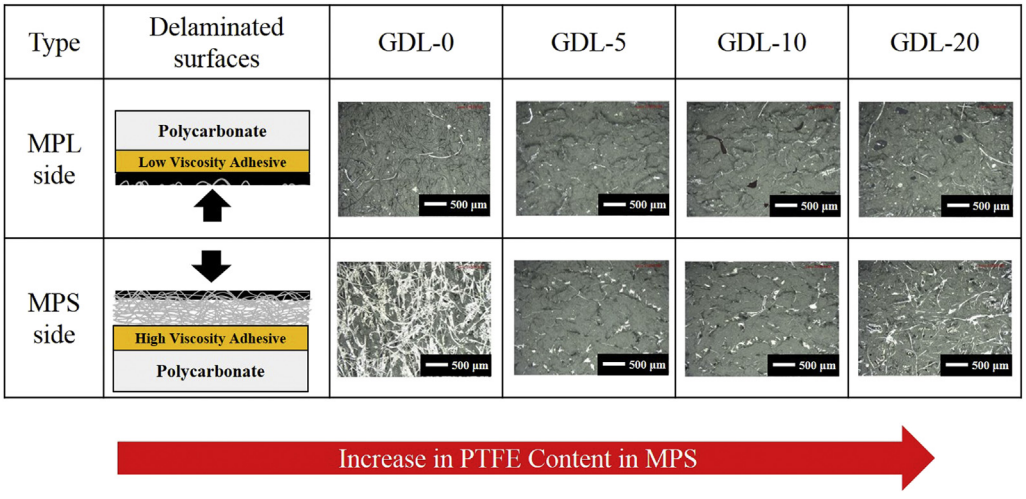

Fig. 5. Delaminated surface characterization observed by OM.

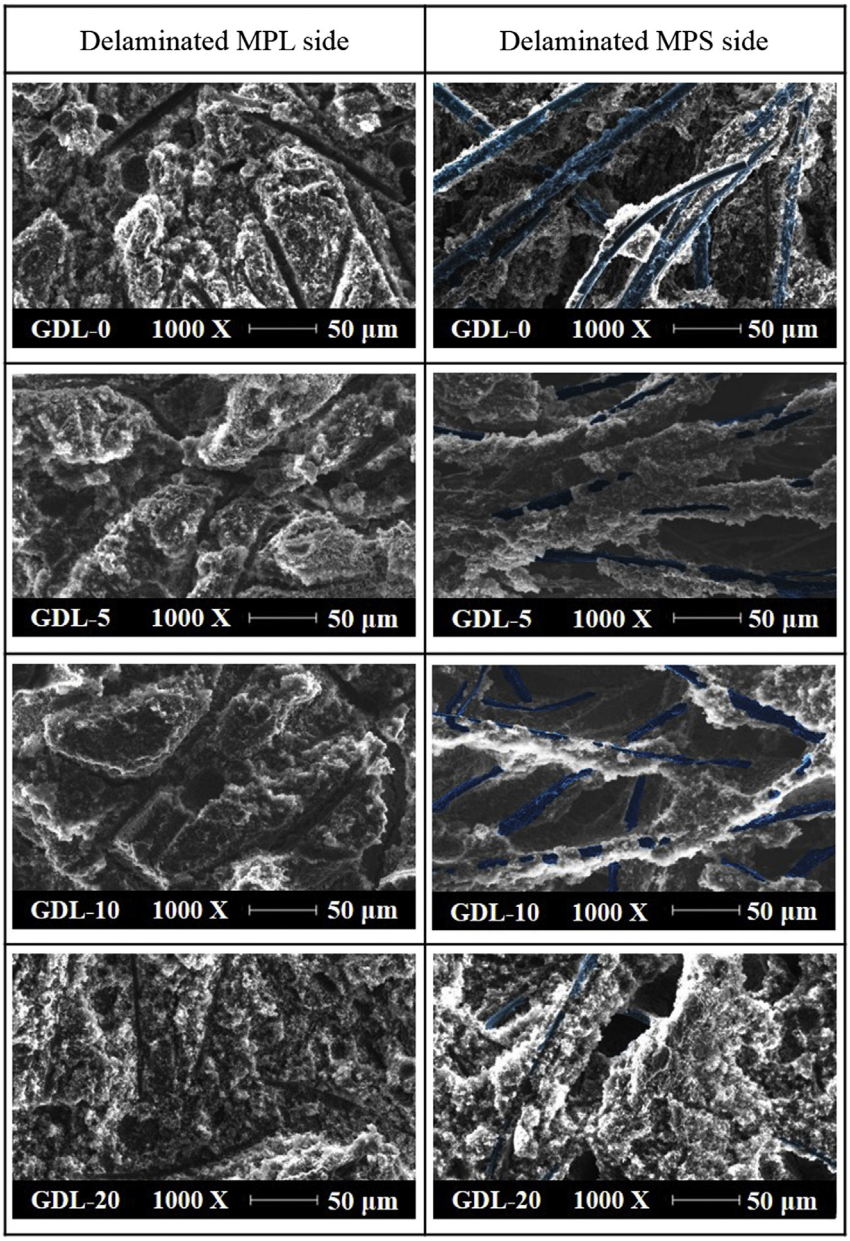

Fig. 6. Delaminated surface characterization observed by SEM.

sides for the GDL-5, GDL-10, and GDL-20 appeared to increase in comparison with those of their corresponding bare MPS surfaces in Fig. 8(b). This was attributed to the more favorable interactions between the MPL and MPS, and thus more MPL residue on the delaminated MPS surfaces for GDL-5, GDL-10, and GDL-20. In Fig. 8(d), it is noteworthy that the delaminated surface of the MPS side of the GDL-0 contained approximately 7.12 wt% fluorine elements despite its PTFE absence on the bare MPS surface (see Fig. 8(b)). This primarily results from the presence of some MPL residues with PTFE on the delaminated MPS sides although the interaction between the MPL and MPS for GDL-0 was poor.

4. Conclusions

The interfacial fracture energy between the MPL and MPS in GDLs is measured quantitatively using DCB tests as a function of various PTFE contents in the MPS. It is observed that the interfacial fracture energy of the GDLs increases gradually with increasing PTFE content in the MPS, which leads to the interfacial fracture energy of the GDL-20 being approximately three times higher than that of the GDL-0. In order to understand the mechanism of the observed fracture behavior in more detail, surface characterizations of the bare and delaminated GDL surfaces after the DCB tests are examined thoroughly using OM, SEM, and EDX. It is found that the GDL-20 had significantly more MPL residue in the MPS than the GDL-0. Thus, it is considered that the GDL-20 exhibits a higher resistance against the external forces exerted during the DCB test because the higher PTFE content in the MPS may facilitate more favorable interactions with the PTFE in the MPL, which leads to higher interfacial fracture energies between the MPL and MPS of the GDL. In contrast, the GDL-0 exhibits an easy separation and removal of the MPL from the MPS during the test because the GDL did not contain PTFE in the MPS, which causes a weak interaction between the MPL and MPS. All surface characterization analysis

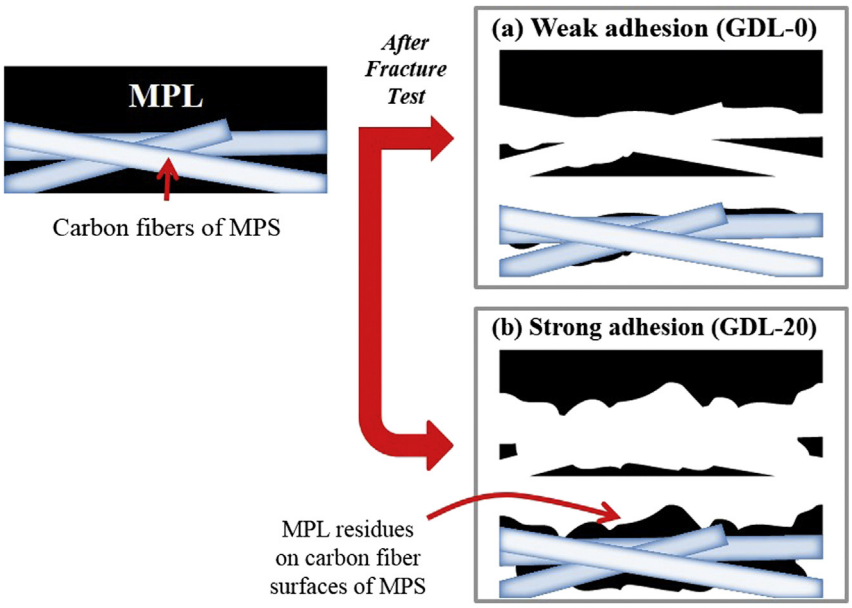

Fig. 7. Debonding mechanisms for the GDLs with (a) weak and (b) strong MPL/MPS adhesion.

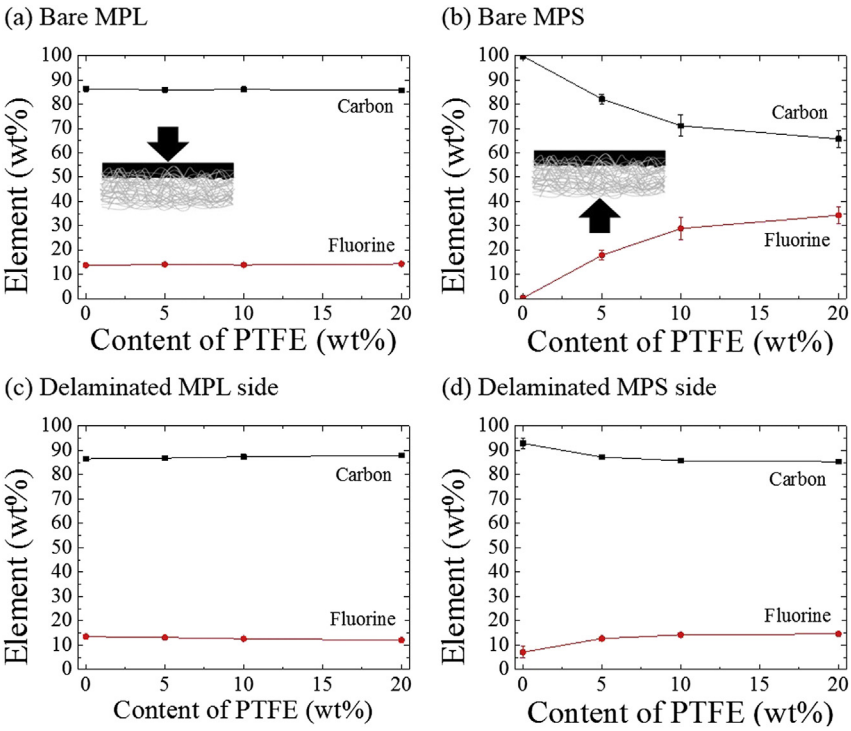

Fig. 8. Delaminated surface characterization by EDX.

results support this mechanism. Therefore, it can be concluded that the quantification of the facture energy of GDL explored in this study could contribute to establishing guidelines for designing more durable and robust GDLs for fuel cell vehicle applications.

Acknowledgments

This work was supported by Hyundai Motor Company. This work was also funded by the Global Frontier R&D Program on Center for Multiscale Energy System (2011–0031569) and the Basic Science Research Program (2012R1A1A1006072) of the National Research Foundation under the Ministry of Science, ICT & Future Planning, Korea.

References

[1] C.-H. Liu, T.-H. Ko, J.-W. Shen, S.-I. Chang, S.-I. Chang, Y.-K. Liao, J. Power Sources 191 (2009) 489–494.
[2] J.-H. Jang, W.-M. Yan, C.-C. Shih, J. Power Sources 161 (2006) 323–332.
[3] H.-K. Lee, J.-H. Park, D.-Y. Kim, T.-H. Lee, J. Power Sources 131 (2004) 200–206.
[4] L. Cindrella, A. Kannan, J. Lin, K. Saminathan, Y. Ho, C. Lin, J. Wertz, J. Power Sources 194 (2009) 146–160.
[5] S. Gamburzev, A.J. Appleby, J. Power Sources 107 (2002) 5–12.

[6] D.E. Curtin, R.D. Lousenberg, T.J. Henry, P.C. Tangeman, M.E. Tisack, J. Power Sources 131 (2004) 41–48.
[7] S. Kim, B.K. Ahn, M. Mench, J. Power Sources 179 (2008) 140–146.
[8] Z. Qi, A. Kaufman, J. Power Sources 109 (2002) 38–46.
[9] K. Han, B.K. Hong, S.H. Kim, B.K. Ahn, T.W. Lim, Int. J. Hydrogen Energy 35 (2010) 12317–12328.
[10] X.L. Wang, H.M. Zhang, J.L. Zhang, H.F. Xu, Z.Q. Tian, J. Chen, H.X. Zhong, Y.M. Liang, B.L. Yi, Electrochim. Acta 51 (2006) 4909–4915.
[11] S. Park, J.-W. Lee, B.N. Popov, Int. J. Hydrogen Energy 37 (2012) 5850–5865.
[12] S. Park, J.-W. Lee, B.N. Popov, J. Power Sources 177 (2008) 457–463.
[13] W.-M. Yan, C.-Y. Hsueh, C.-Y. Soong, F. Chen, C.-H. Cheng, S.-C. Mei, Int. J. Hydrogen Energy 32 (2007) 4452–4458.
[14] J.T. Gostick, M.A. Ioannidis, M.W. Fowler, M.D. Pritzker, Electrochem. Commun. 11 (2009) 576–579.
[15] S. Escribano, J.-F. Blachot, J. Ethève, A. Morin, R. Mosdale, J. Power Sources 156 (2006) 8–13.
[16] U. Pasaogullari, C. Wang, J. Electrochem. Soc. 151 (2004) A399–A406.
[17] J. Benziger, J. Nehlsen, D. Blackwell, T. Brennan, J. Itescu, J. Memb. Sci. 261 (2005) 98–106.
[18] J. Ge, A. Higier, H. Liu, J. Power Sources 159 (2006) 922–927.
[19] Y. Li, D.A. Dillard, S.W. Case, M.W. Ellis, Y.-H. Lai, C.S. Gittleman, D.P. Miller, J. Power Sources 194 (2009) 873–879.
[20] E. Cho, J.-J. Ko, H.Y. Ha, S.-A. Hong, K.-Y. Lee, T.-W. Lim, I.-H. Oh, J. Electrochem. Soc. 150 (2003) A1667–A1670.
[21] K. Han, B.K. Hong, S.H. Kim, B.K. Ahn, T.W. Lim, Int. J. Hydrogen Energy 36 (2011) 12452–12464.
[22] C. Lee, W. Mérida, J. Power Sources 164 (2007) 141–153.
[23] R. Jia, S. Dong, T. Hasegawa, J. Ye, R.H. Dauskardt, Int. J. Hydrogen Energy 37 (2012) 6790–6797.
[24] M. Ismail, T. Damjanovic, D. Ingham, M. Pourkashanian, A. Westwood, J. Power Sources 195 (2010) 2700–2708.
[25] Website of SGL Technologies GmBH, Germany. Available: http://www. http://www.sglgroup.com/(accessed July 2014).
[26] S.R. Dupont, M. Oliver, F.C. Krebs, R.H. Dauskardt, Sol. Energy Mater. Sol. Cells 97 (2012) 171–175.
[27] R.J. Hohlfelder, D.A. Maidenberg, R.H. Dauskardt, Y. Wei, W. Hutchinson, J. Mater. Res. 16 (2001) 243–255.
[28] M. Kanninen, Int. J. Fract. 9 (1973) 83–92.
[29] T.S. Kim, T. Konno, R.H. Dauskardt, Acta Mater. 57 (2009) 4687–4696.
[30] T.S. Kim, N. Tsuji, K. Matsushita, N. Kobayashi, D. Chumakov, H. Geisler, E. Zschech, R.H. Dauskardt, J. Appl. Phys. 104 (2008) 074113–074116.
[31] I. Lee, S. Kim, J. Yun, I. Park, T.S. Kim, Nanotechnology 23 (2012) 485704.
[32] K.S. Wu, M.M. Stefik, K. Ananthapadmanabhan, R.H. Dauskardt, Biomaterials 27 (2006) 5861–5870.
[33] K.S. Wu, W.W. van Osdol, R.H. Dauskardt, Biomaterials 27 (2006) 785–795.
[34] T. Yoon, W.C. Shin, T.Y. Kim, J.H. Mun, T.S. Kim, B.J. Cho, Nano Lett. 12 (2012) 1448–1452.